

BENDING AND SPRINGBACK PREDICTION METHOD BASED ON MULTI-SCALE FINITE ELEMENT ANALYSES FOR HIGH BENDABILITY AND LOW SPRINGBACK SHEET GENERATION

T. HONDA^{*}, H. KURAMAE[†], H. MORIMOTO^{†2},
Y. MORITA^{†3}, Y. NAKAMURA^{†4}, T. OHATA^{†4}, E. NAKAMACHI^{†3}

^{*} Graduate School, Department of Mechanical Engineering, Doshisha University,
Kyotanabe, Kyoto, 610-0394, Japan e-mail: dmm0006@mail4.doshisha.ac.jp

[†]Osaka Institute of Technology, 5-16-1, Omiya, Asahi-ku, Osaka, Osaka, 535-8585, Japan
e-mail: kuramae@dim.oit.ac.jp

^{†2}Furukawa Electric Co. LTD., 2-4-3, Okano, Nishi-ku, Yokohama, 220-0073, Japan
e-mail: mr840991@mr.furukawa.co.jp

^{†3}Doshisha University, Kyotanabe, Kyoto, 610-0394, Japan
e-mail: ymorita@mail.doshisha.ac.jp, enakamac@mail.doshisha.ac.jp,

^{†4}Osaka Sangyo University, 3-1-1, Nakagaichi, Daito, Osaka, 574-8530, Japan
e-mail: nkmr@mech.osaka-sandai.ac.jp

Key words: Computational Plasticity, Forming Process, Composites, Nano-mechanics.

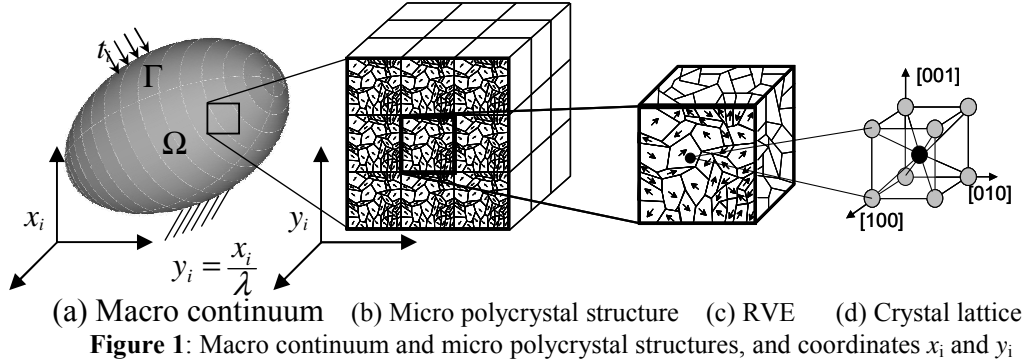
Abstract. *In this study, a sheet bendability and springback property evaluation technology through bending test simulations is newly developed using our multi-scale finite element analysis code, which is based on the crystallographic homogenization method.*

1 INTRODUCTION

In this study, we develop the bendability and the springback prediction analysis code for an optimum crystal texture design scheme to generate ideal copper alloy sheet for the electric devices. Recently, the electronic components, such as connector and switch, have been downsized because of narrow pitch packaging of electric components. Therefore, the copper alloy sheet (Corson alloy (Cu-Si-Ni) or phosphor bronze (Cu-Sn-P)) which is mainly used for electro-mechanical device is required better bendability and accurate forming property. Macroscopic material properties of sheet metals such as the bendability and the formability strongly depend on the microscopic polycrystal morphologies. Furthermore, it is considered that process design analyses to generate an optimum texture for the bendability are available method. In this study, a dynamic explicit crystallographic homogenized FE code [1-4] is applied to simulate the bending test problems of copper alloy sheet metals to predict the bendability and the springback property.

2 FUNDAMENTAL EQUATIONS FOR THE MICRO AND MACRO STRUCTURES

2.1 Crystallographic Homogenization Procedure



We introduce both microscopic and macroscopic coordinate systems so the physical quantities are represented by two different length scales; one is x in the macroscopic region Ω and the other is y ($=x/\lambda$) in the microscopic region Y as shown in Fig. 1. The equations in the microscopic and macroscopic levels are derived by employing defined velocities, \dot{U}_i and \dot{u}_i [1].

The equation of the virtual power principle of the micro polycrystalline structure is expressed as:

$$\int_V \rho \dot{u}_i(x, y) \delta \dot{u}_i(x, y) dV + \int_V \nu \dot{u}_i(x, y) \delta \dot{u}_i(x, y) dV = - \int_V \sigma_{ij} \delta \dot{u}_{i,j}(x, y) dV, \quad (1)$$

$$\dot{\delta u}_i(x, y) = 0 : \text{ on the boundary of region } Y, \quad (2)$$

where ρ and ν mean the mass density and the viscosity coefficient, respectively. By solving the governing equation, Eq. (1), we obtain the Cauchy stresses σ_{ij} . The macroscopic Cauchy stress tensor, which means the homogenized stress tensor, σ_{ij}^H is obtained by averaging Cauchy stresses in microstructure as follows:

$$\sigma_{ij}^H = \langle \sigma_{ij} \rangle = \frac{\sum_{e=1}^{N_e} \left(\sum_{G=1}^{N_G} |J_G| \sigma_{ij}^G \right)}{\sum_{e=1}^{N_e} |J_e|}, \quad (3)$$

where σ_{ij} is Cauchy stress at Gaussian integration point G of a finite element in the microscopic region, J_G^H is the Jacobian at the integration point, N_G is the total number of integration points.

We introduced the homogenized stress σ_{ij}^H and then formulate the virtual power equation of the macro-continuum as follows:

$$\begin{aligned}
& \int_{\Omega} \rho \ddot{U}_i(x) \delta \dot{U}_i(x) d\Omega + \int_{\Omega} \nu \dot{U}_i(x) \delta \dot{U}_i(x) d\Omega \\
& = \int_{\sigma} \bar{T}_i \delta \dot{U}_i(x) d\Gamma - \int_{\Omega} \sigma_{ij}^H(x) \frac{\partial \delta \dot{U}_i(x)}{\partial x_j} d\Omega
\end{aligned} \tag{4}$$

where $\Omega, \Gamma_{\sigma}, \bar{f}_i$ and \bar{T}_i are the volume, force boundary surface, the body force and the external surface force, respectively.

2.2 A two-scale "dynamic-explicit" finite element formulation

In this section, the "dynamic-explicit" homogenized elastic/crystalline viscoplastic FE procedure is shown. The eight nodes iso-parametric solid element is used for both macro continuum and micro polycrystal structure. We employ the shape functions for macro and micro 8 nodes iso-parametric solid finite elements, as follows;

$$N_{\alpha}^0 = \frac{1}{8} (1 + \xi_1 \xi_{1\alpha}) (1 + \xi_2 \xi_{2\alpha}) (1 + \xi_3 \xi_{3\alpha}) : \text{for macro region} \tag{5}$$

$$N_{\alpha}^{[p,q]} = \frac{1}{8} (1 + \varsigma_1 \varsigma_{1\alpha}^{[p,q]}) (1 + \varsigma_2 \varsigma_{2\alpha}^{[p,q]}) (1 + \varsigma_3 \varsigma_{3\alpha}^{[p,q]}) : \text{for micro region} \tag{6}$$

Where, ξ_i is the natural coordinate, which employs the macro coordinate x_i , and ς_i to y_i . The superscript "0" corresponds to the value in the macro region, and "1" the micro region. q and p mean q -th finite element defined in the base cell "Y", which means RVE micro polycrystal structure, of the corresponding p -th macro finite element, as shown in Fig. 1.

The velocity gradients at the macroscopic and microscopic levels are derived as follows,

$$L_{ij} = \frac{\partial \dot{U}_i}{\partial x_j} = \sum_{\alpha=1}^8 \frac{\partial N_{\alpha}^0}{\partial x_j} \dot{U}_{i\alpha} = \sum_{\alpha=1}^8 N_{\alpha,j}^0 \dot{U}_{i\alpha}; \quad \dot{U}_i = \sum_{\alpha=1}^8 N_{\alpha}^0 \dot{U}_{i\alpha} \tag{7}$$

$$l_{ij} = \frac{\partial \dot{u}_i}{\partial y_j} = \sum_{\beta=1}^8 \frac{\partial N_{\beta}^{[p,q]}}{\partial y_j} \dot{u}_{i\beta} = \sum_{\beta=1}^8 N_{\beta,j}^{[p,q]} \dot{u}_{i\beta}; \quad \dot{u}_i = \sum_{\beta=1}^8 N_{\beta}^{[p,q]} \dot{u}_{i\beta} \tag{8}$$

where, α and β mean the finite element node number of macro and micro elements, p and q mean the same as defined in Eq. (6).

Substituting Eq. (7) into the virtual power equation (4), a FE equation of motion in the macro region Ω_e is obtained by using the Gaussian integration calculations.

Finally, the FE equation for the whole macro continuum region is calculated as,

$$\sum_{\beta=1}^8 M_{\alpha\beta}^0 \ddot{U}_{j\beta} + \sum_{\beta=1}^8 C_{\alpha\beta}^0 \dot{U}_{j\beta} = P_{j\alpha}^0 - F_{j\alpha}^0 \tag{9}$$

where,

$$\begin{aligned}
M_{\alpha\beta}^0 &= \sum_{e=1}^T \int_{\Omega_e} \rho N_{\alpha}^0 N_{\beta}^0 d\Omega, & C_{\alpha\beta}^0 &= \sum_{e=1}^T \int_{\Omega_e} \nu N_{\alpha}^0 N_{\beta}^0 d\Omega, \\
P_{j\alpha}^0 &= \sum_{e=1}^T \int_{\Gamma_e} N_{\alpha}^0 \bar{T}_j d\Gamma, & F_{j\alpha}^0 &= \sum_{e=1}^T \int_{\Omega_e} N_{\alpha,j}^0 \sigma_{ij}^H d\Omega
\end{aligned} \tag{10}$$

Those are the mass, the viscosity, the external force and the internal force terms. "e" means a

macro finite element, T the total number of finite elements in the macro continuum region, α the node number in the whole macro continuum region.

Next, substituting Eq. (8) into Eq. (1), a FE equation of motion in the micro region Y_e is obtained by using the same derivation process as in the macro region. A total “micro” FE equation of motion is given by,

$$\sum_{\beta=1}^8 M_{\alpha\beta}^{[p,q]} \ddot{u}_{j\beta} + \sum_{\beta=1}^8 C_{\alpha\beta}^{[p,q]} \dot{u}_{j\beta} = -F_{j\alpha}^{[p,q]} \quad (11)$$

where,

$$M_{\alpha\beta}^{[p,q]} = \sum_{e=1}^{MT} \int_{Y_e} \rho N_{\alpha}^{[p,q]} N_{\beta}^{[p,q]} dY, C_{\alpha\beta}^{[p,q]} = \sum_{e=1}^{MT} \int_{Y_e} \nu N_{\alpha}^{[p,q]} N_{\beta}^{[p,q]} dY, F_{j\alpha}^{[p,q]} = \sum_{e=1}^{MT} \int_{Y_e} N_{\alpha,j}^{[p,q]} \sigma_{il}^{[p,q]} dY \quad (12)$$

MT means the total number of micro finite elements in the whole micro structure region Y , and α the node number in the whole micro region. On the boundary surface of the micro region Y , the incremental displacement is assigned, which is calculated by using the velocity gradient at the corresponding integration point of macro element. We employ the conventional time integration algorithm, “Central difference method”, to solve both equations of motion [5-7]. By using the displacement at the time step $t + \Delta t$, the strain increments and Cauchy stress increments are calculated in the whole “micro” finite elements of the micro polycrystal structure. Then, the “homogenized” Cauchy stress is obtained at every integration point of “macro” finite elements.

2.3 Elastic/Crystalline Viscoplastic Constitutive Equation

We employed the strain rate dependent crystal plasticity constitutive equation for micro analysis[8-13]. The crystalline viscoplastic shear strain rate $\dot{\gamma}^{(a)}$ of the power law form defined on the slip system a is expressed as follow:

$$\dot{\gamma}^{(a)} = \dot{\gamma}_0^{(a)} \left[\frac{\tau^{(a)}}{g^{(a)}} \right] \left[\left| \frac{\tau^{(a)}}{g^{(a)}} \right| \right]^{\frac{1}{m}-1}, \quad (13)$$

where $\tau^{(a)}$ is the resolved shear stress, $g^{(a)}$ is the reference shear stress, $\dot{\gamma}_0^{(a)}$ is the reference shear strain rate, and m is the coefficient of strain rate sensitivity. In this study, $\dot{\gamma}_0^{(a)} = 0.033$ and $m = 0.01$ is employed in FCC metal, respectively.

The hardening evolution equation of the reference shear stress $g^{(a)}$ is given by

$$\dot{g}^{(a)} = \sum_{b=1}^N h_{ab} |\dot{\gamma}^{(b)}| \quad (14)$$

where N is the total number of slip systems, for the FCC crystal $N = 12$. The hardening coefficients h_{ab} for the n -th power equation are expressed as follows:

$$h_{ab} = q_{ab} \frac{d\tau(\gamma)}{d\gamma} + (1 - q_{ab}) \frac{d\tau(\gamma)}{d\gamma} \delta_{ab} \quad (15)$$

$$\frac{d\tau(\gamma)}{d\gamma} = h(\gamma) = h_0 n C \{C(\gamma_0 + \gamma)\}^n \quad (16)$$

where the matrix q_{ab} is introduced to describe the self and latent hardenings. γ is the accumulated shear strain over all the slip systems, h_0 is the initial hardening modulus and n and C is the hardening exponent and the hardening coefficient, respectively. These values are determined by the parameter identification calculation through the comparison with the experimental results [1].

The objective rate of Cauchy stress $\dot{\sigma}_{ij}^*$ is employed in the rate type elastic/visco crystal plasticity constitutive equation as given by,

$$\dot{\sigma}_{ij}^* = C_{ijkl}^e D_{kl} - \sum_a R_{ij}^{(a)} \dot{\gamma}^{(a)} \quad (17)$$

where C_{ijkl}^e is a fourth order tensor of elastic moduli and D_{kl} is the rate of deformation tensor. The detail formulation procedure can be found in the authors' paper [1].

3 MULTI-SCALE ANALYSES OF BENDING PROCESS

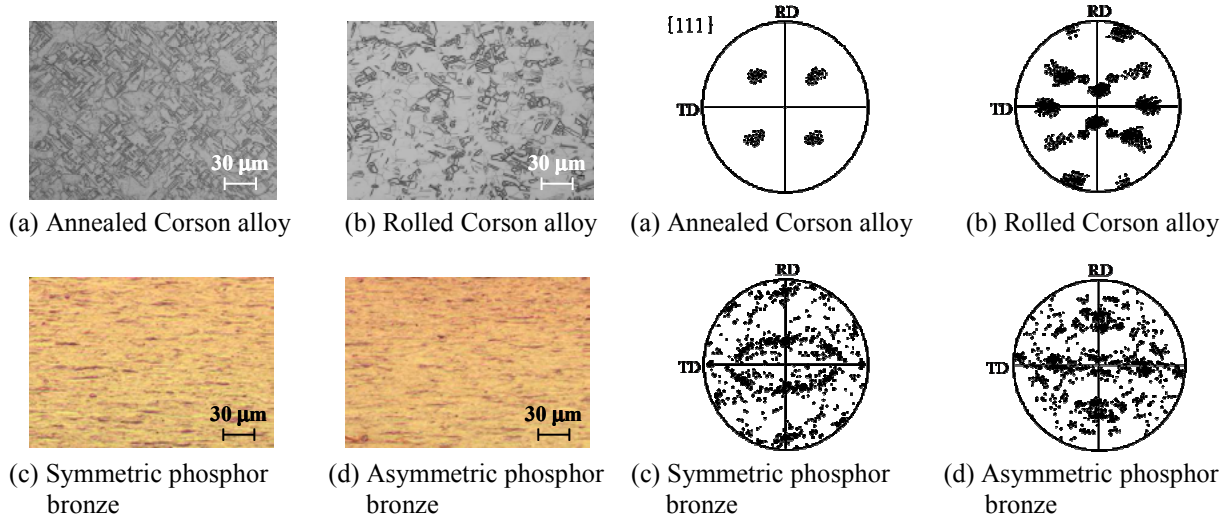


Figure 2: Observation of crystalline grain orientation distribution by using optical microscope

Figure 3: Crystal textures of four polycrystal copper alloys

Table 1: Statistically ratio of preferred orientation of four copper alloys

Crystal orientation	Component	Ratio (%)			
		Cu-Ni-Si		Cu-Sn-P	
		Annealed alloy	Rolled alloy	Symmetric alloy	Asymmetric alloy
{112}(111)	Copper	0.00	1.95	1.17	0.00
{123}(634)	S	0.00	4.66	0.00	0.00
{110}(112)	Brass	0.00	0.00	5.11	0.00
{001}(100)	Cube	64.23	0.00	0.01	0.04
{001}(110)	α -fiber	0.00	0.00	0.00	1.48
{111}(110)	γ -fiber	0.00	0.00	0.00	0.41
{111}(112)	γ -fiber	0.00	0.00	0.03	2.83

We employed four copper alloys of Corson alloy and phosphor bronze (Cu-Sn-P) in the multi-scale FE analyses, such as a full annealed alloy and an annealed and rolled alloy of Corson alloy, named “Annealed Corson alloy” and “Rolled Corson alloy,” and a symmetric and an asymmetric rolled alloy of phosphor bronze (Cu-Ni-Si), named as “Symmetric phosphor bronze” and “Asymmetric phosphor bronze.” Figure 2 shows optical microscope photos of the crystal grain distribution of four copper alloys. In this study, the crystal orientations measured by SEM-EBSD were introduced into integration points of the micro-finite elements of the representative volume element (RVE). In the case of Corson alloy, we measured the crystal orientation distribution on the surface by using SEM-EBSD and calculate to find a minimum number of crystal orientations (grains) to characterize the crystal plasticity constitutive law, which satisfied the periodicity of crystallographic morphology and constitutive law. Finally we found that 216 crystal orientations were enough for RVE – micro-FE model -. We used SEM-EBSD measured orientations for “Annealed Corson alloy” and “Rolled Corson alloy.” On the other hand, the rolled phosphor bronze is characterized as the extremely high strained crystal and then the difficulty of measurement. So we measure the crystal orientation distributions of before rolling and carried out multi-scale FE analyses of the symmetric and asymmetric rolling to obtain the crystal orientation distributions, which were used for “Symmetric phosphor bronze” and “Asymmetric phosphor bronze.” Figure 3 shows these four initial crystal orientation distributions of RVEs and Table 1 shows the probability ratio of preferred orientation of four copper alloys. “Annealed Corson alloy” has the Cube orientation as the dominant texture, “Rolled Corson alloy” the S orientation, “Symmetric phosphor bronze” the Brass orientation, and “Asymmetric phosphor bronze” the $\{001\}\langle 110 \rangle$ orientation, respectively. These four textures, characterized by 216 crystal orientations, were assigned to the integration point of the micro FE models – RVEs – for multi-scale FE analyses of the sheet bending process.

3.1 Material identification

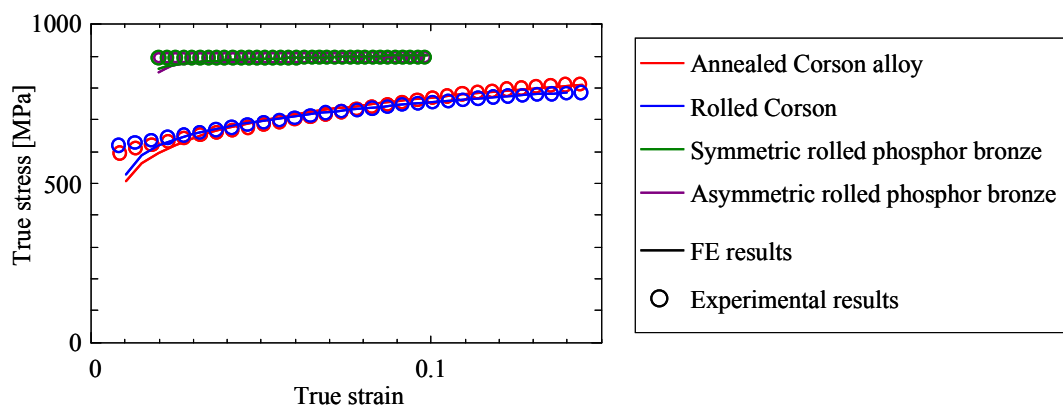


Figure 4: Stress-strain curves obtained by experiments and FE analyses using RVE-FE model

Table 2: Material properties of crystal plasticity constitutive model

	Annealed Corson alloy	Rolled Corson alloy	Symmetric phosphor bronze	Symmetric phosphor bronze
n	0.13	0.08	0.01	0.01
τ_0 [MPa]	179.8	170.0	276.0	285.0
h_0 [MPa]	197.2	164.0	29.0	47.0

Three crystal material parameters, τ_0 , h_0 and n , of the hardening evolution equation (16) were identified by the least square method using FE simulation results of the uni-axial tension tests through the comparison with the experimental results. Figure 4 shows stress-strain curves obtained by the experiments of tensile test in the rolling direction (RD) and the multi-scale FE results by employing 27 (= 3×3×3) micro FEs with 216 Gaussian integration points. Table 2 summarizes the crystal plastic material properties for four sheet metals.

3.2 Bendability and springback property index

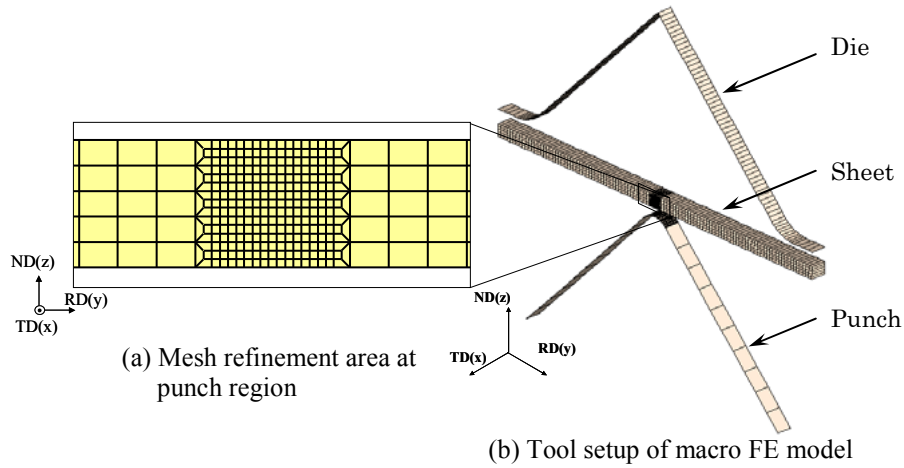


Figure 5: Tool setup and mesh refinement at punch region for FE analysis of bending test problem

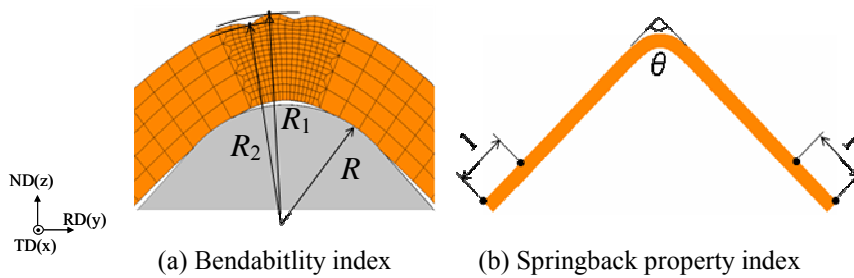


Figure 6: Definition of bending index

The bending tests were simulated by using the multi-scale FE code, which can be featured as the dynamic explicit crystallographic homogenized finite element methods -. Figure 5 (b) shows tool setup for the problem. The setup of the macro FE model consists of the die, punch and sheet metal. The die and punch is modeled as the rigid bodies for “V- bending”. The FE model of macro-continuum as the sheet metal employed 8-node iso-parametric solid element,

and a total number of finite elements was 765. The mesh division pattern of the sheet metal was composed of two regions, such as the fine and coarse regions. The fine mesh can predict the strain distribution and the shear band formations precisely, but it increases the computation time required to complete the simulation. Thus, we employed the fine meshes for the stress concentration and critical regions. Figure 5 (a) shows the fine FE mesh division region, which locates on the punch region, where the large deformations, high stresses and high strains could be occurred. The FE model of microstructure as the RVE polycrystal model was divided into 27 ($= 3 \times 3 \times 3$) 8-node solid elements with 216 crystal orientations.

We defined a surface wrinkle w as the macroscopic bendability index, and the springback angle $\Delta\theta$ as the springback index as follows:

$$w = \frac{R_1 - R_2}{t} \times 100(\%) \quad (17)$$

$$\Delta\theta = \theta_2 - \theta_1 \quad (18)$$

where t is the initial sheet thickness, R_1 and R_2 are distance between top and bottom of the wrinkle from punch center and θ_1 and θ_2 are angles before and after the springback as shown in Fig. 6. The less value of w , the greater the bendability the sheet metal has. The less value of $\Delta\theta$, the greater the springback property the sheet metal has.

3.3 Bending process analyses

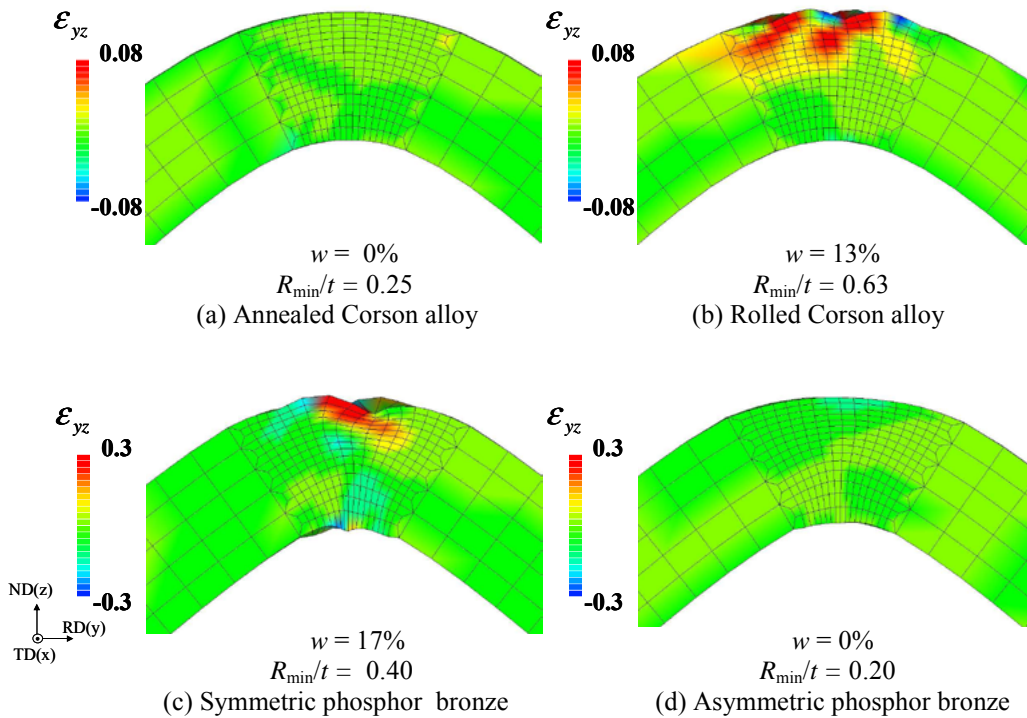
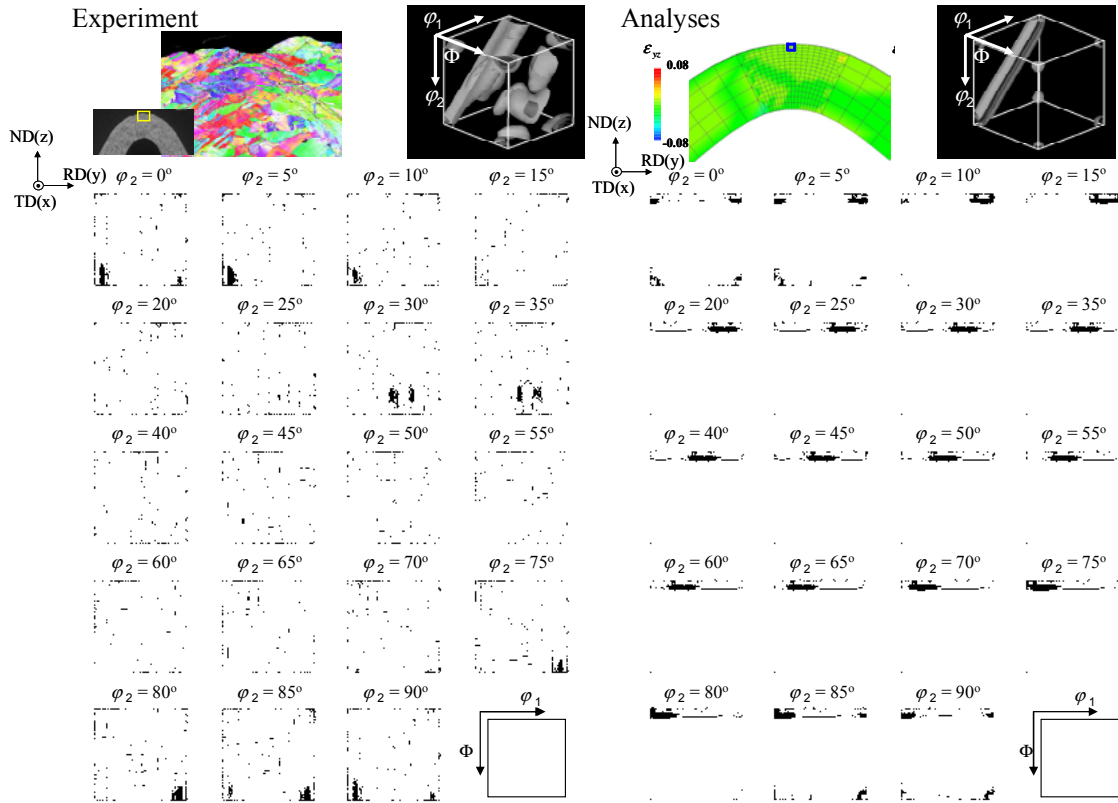
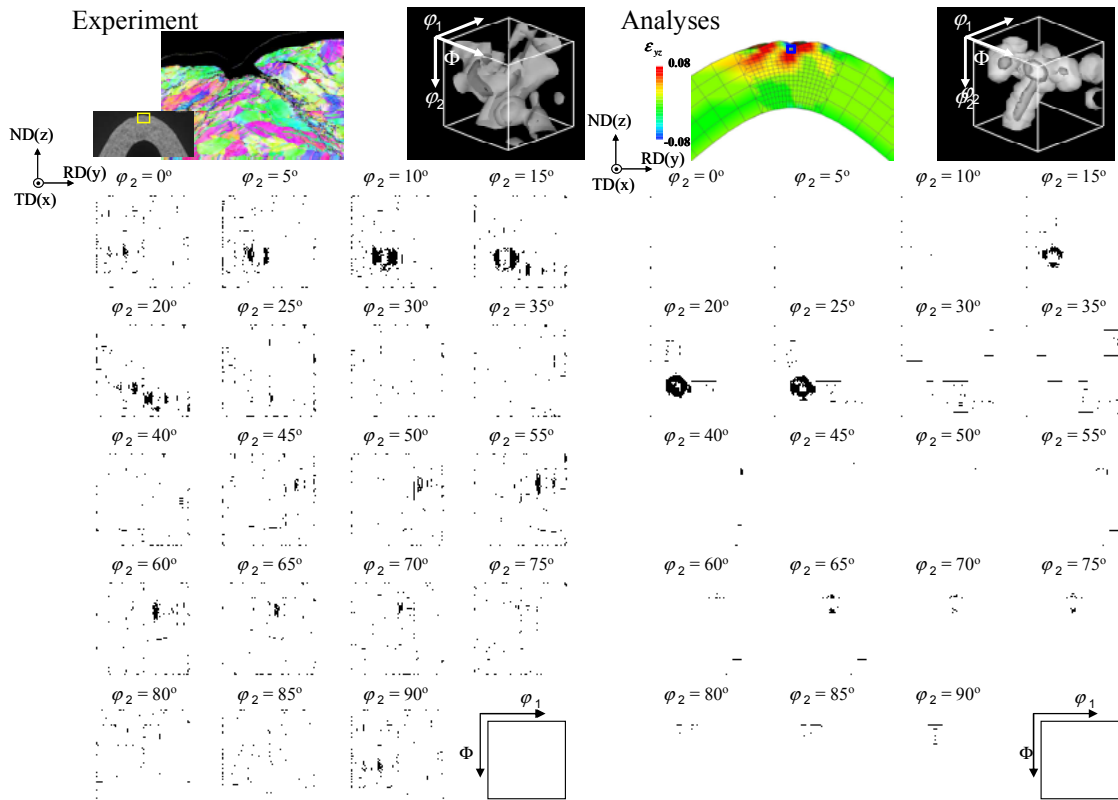


Figure 7: Comparison of shear strain distribution in four polycrystalline copper alloys



(a) Annealed Corson alloy



(b) Rolled Corson alloy

Figure 8: Comparison of macro deformation and ODF analyses between experiment and analyses

Figure 7 shows comparisons of the shear strain distribution and w value by using the results of our multi-scale FE analyses and R_{\min} / t value by using the results of experiments. The smaller the R_{\min} / t value, the greater the bendability the sheet metal has. In the numerical results, Annealed Corson alloy and Asymmetric phosphor bronze show a high bendability because of low w value and uniform strain distributions. On the other hand, Rolled Corson alloy and Symmetric phosphor bronze show poor bendability because of high w value and the shear band formation. In the experimental results, Annealed Corson alloy and Asymmetric phosphor bronze also show high bendability. Therefore, we confirmed that the numerical results show good agreement with the experimental results.

In the Corson alloy, we compare macroscopic plastic deformation and microscopic texture evolution between experimental results and numerical results in Annealed Corson alloy and in Rolled Corson alloy, in detail. Figure 8 shows the comparison between experimental results and numerical results of macro deformation and micro ODF results in the case of two Corson alloys. In the case of experiment, we measured the crystal orientation distribution by using SEM-EBSD and compared of ODF results in the yellow square. In the macro deformation, in the case of Annealed Corson alloy show uniform straining both experiment and analyses. On the other hand, in the case of Rolled Corson alloy shows shear band formation in experimental and also shows shear strain localization in the analysis. Therefore, in macro deformation the numerical results show good agreement with the experimental results. In the texture evolution after deformation, in the case of Annealed Corson alloy, Cube orientations still remain both experimental results and numerical results after bending. This means that uniform slip deformation occurs. Therefore Cube dominant texture shows high bendability. On the other hand, Rolled Corson alloy shows concentrate toward the Copper orientation both experimental results and numerical results after bending. Comparison of ODF results between experiment and multi-scale FE analysis agrees very well. Therefore, our analysis code can predict macroscopic bending deformation and microscopic texture evolution precisely, so our method is available method in bending process.

3.4 Springback analyses

We analyzed the springback after the bending by removing the die. Figure 9 shows a comparison with the rolling direction stress distributions before and after the springback. After unloading, compared with before unloading, four copper alloy sheets show stress relaxation. This means that springback finished completely. Rolled Corson alloy and Symmetric phosphor bronze which have poor bendability components show smaller $\Delta\theta$ value than Annealed Corson alloy and symmetric phosphor bronze which have high bendability components. Furthermore, FE analyses reveal that high bendability material does not necessarily have high springback property. It is considered that process design to generate optimum texture in bendability and springback property are available method.

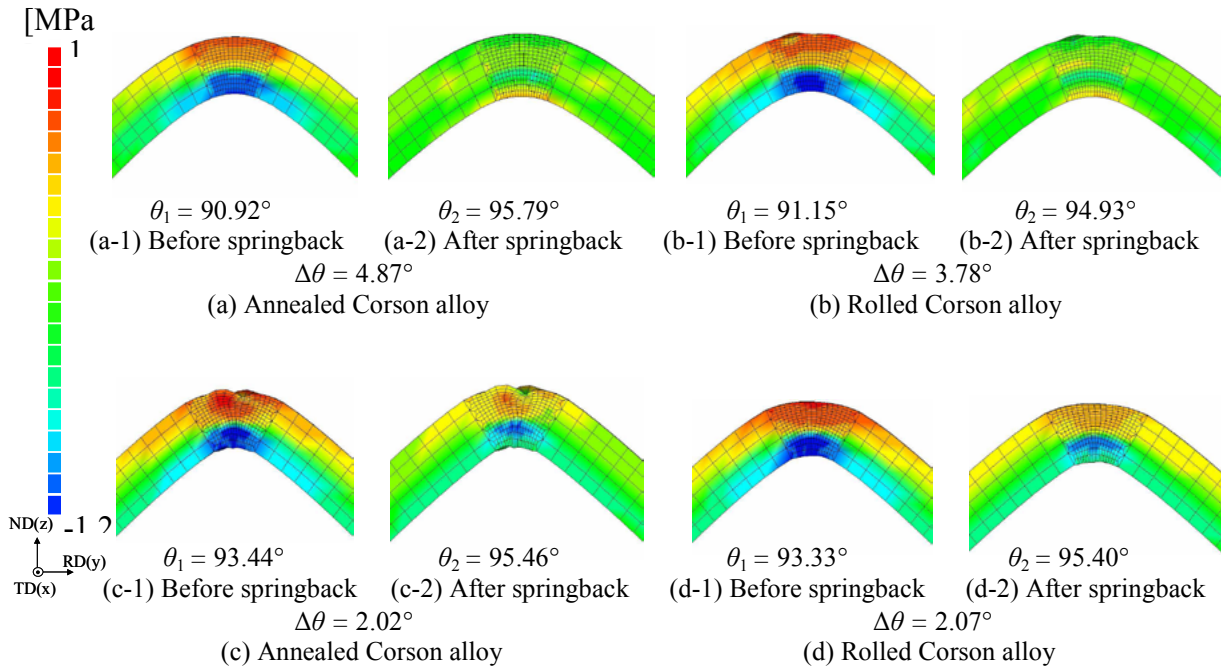


Figure 9: Comparison of RD stress distribution in four polycrystal copper alloys before and after springback

4 CONCLUSIONS

In this study, crystalline homogenized finite element procedure, based on the dynamic explicit method, was applied to analyze bending test problem for copper alloy bendability assessment. We studied relationship between the crystal orientation and bendability by using seven single crystal models. We compared between experimental results and numerical results by polycrystal Corson alloy and phosphor bronze to verify availability of our multi-scale code. The macro- and micro-finite element analyses reveal the bendability as follows:

- In our multi-scale bending analyses, Annealed Corson alloy which has Cube orientation dominant texture and Asymmetric phosphor bronze which has $\{001\}\langle 110 \rangle$ orientation dominant texture show high bendability. On the other hand, Rolled Corson alloy which has S orientation dominant texture and Symmetric phosphor bronze which has Brass orientation dominant texture show poor bendability. These result show good agreement with experimental results.
- In Corson alloy, in the case of Annealed Corson alloy which has Cube orientation dominant texture, Cube orientations still remain. On the other hand, Rolled Corson alloy which has S orientation dominant texture shows concentrate toward the Copper orientation. These result also show good agreement with experimental results.
- Annealed Corson alloy and Asymmetric phosphor bronze which has high bendability texture show low springback property. On the other hand, Rolled Corson alloy and Symmetric phosphor bronze show high springback property. Furthermore, FE analyses revealed that high bendability material does not necessarily have high springback property.

REFERENCES

- [1] E. Nakamachi, N.N. Tam, H. Morimoto, Multi-scale finite element analyses of sheet materials by using SEM-EBSD measured crystallographic RVE models, *Int. J. Plasticity*, 23 (2007) 450-489.
- [2] E. Nakamachi, C.L. Xie, H. Morimoto, K. Morita, N. Yokoyama, Formability assessment of FCC aluminum alloy sheet by using elastic/crystalline viscoplastic finite element analysis, *Int. J. Plasticity*, 18 (2002) 617-632.
- [3] E. Nakamachi, K. Hiraiwa, H. Morimoto, M. Harimoto, Elastic/crystalline viscoplastic finite element analyses of single- and poly-crystal sheet deformations and their experimental verification, *Int. J. Plasticity*, 16 (2000) 1419-1441.
- [4] E. Nakamachi, X. Dong, Study of texture effect on sheet failure in a limit dome height test by using elastic/crystalline viscoplastic finite element analysis, *J. App. Mech.*, 64 (1997) 519-524.
- [5] E.R. Homer, B.L. Adams, R.H. Wagoner, Recovering grain-boundary inclination parameters through oblique double sectioning, *Metallurgical and Materials Trans. A*, 38A (2007) 1575-1586.
- [6] J.W. Signorelli, M.A. Bertinetti, P. A. Turner, Prediction of forming limit diagrams using a rate-dependent polycrystal self-consistent plasticity model, *Int. J. Plasticity*, 25 (2009) 1-25.
- [7] O. Diard, S. Leclercq, G. Rousselier, G. Cailletaud, Evaluation of finite element based analysis of 3D multicrystalline aggregates plasticity Application to crystal plasticity model identification and the study of stress and strain fields near grain boundaries, *Int. J. Plasticity*, 21 (2005) 691-722.
- [8] A. Needleman, Finite element for finite strain plasticity problems, *Proc. The Workshop on Plasticity of Materials at Finite Strain*, 1981, 1-11.
- [9] R.J. Asaro, Crystal plasticity, *J. App. Mech.*, 50 (1983) 921-934.
- [10] R.J. Asaro, A. Needleman, Texture development and strain hardening in rate dependent polycrystals, *Acta Metallurgica*, 33 (1985) 923-953.
- [11] J. Pan, J.R. Rice, Rate sensitivity of plastic flow and implications for yield-surface vertices, *Int. J. Solid and Struct.*, 19 (1983) 973-987.
- [12] Y. Zhou, K.W. Neale, L.S. Tóth, A modified model for simulating latent hardening during the plastic deformation of rate-dependent FCC polycrystals, *Int. J. Plasticity*, 9 (1993) 961-978.
- [13] J. Harder, Crystallographic model for the study of local deformation processes in polycrystals, *Int. J. Plasticity*, 15 (1999) 605-624.